Understanding Energy Transfer Mechanisms for Tunable Emission of Yb^{3+}-Er^{3+} Codoped GdF_3 Nanoparticles: Concentration-Dependent Luminescence by Near-Infrared and Violet Excitation

Dekang Xu,[†] Chufeng Liu,[†] Jiawei Yan,[†] Shenghong Yang,[†] and Yueli Zhang*[,†,‡]

[†] State Key Laboratory of Optoelectronic Materials and Technologies, School of Physics and Engineering, Sun Yat-Sen University, Guangzhou 510275, People's Republic of China

[‡] State Key Laboratory of Crystal Material, Shandong University, Jinan 250100, People's Republic of China

* Corresponding Author: stszyl@mail.sysu.edu.cn

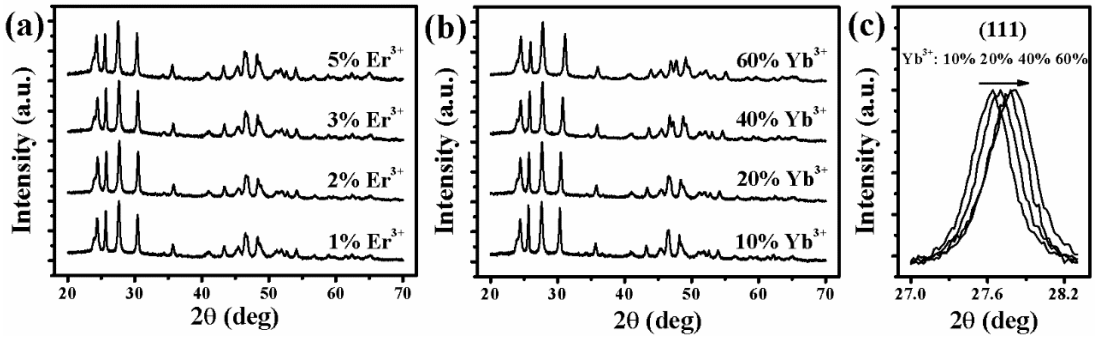

Figure S1 XRD patterns of GdF_3 with (a) different Er^{3+} dose and (b) different Yb^{3+} dose. (c) Magnification of (111) diffraction peak of samples with different Yb^{3+} dose.

The structure of all samples are typical orthorhombic phase with Pnma space group. From Fig. 1(a), the structures of the samples doped with different Er^{3+} concentration are almost unchanged, due to the small radii difference of Gd^{3+} (0.935 Å) ion and Er^{3+} (0.89 Å) ion and small amount of doping. However, the structures of samples with different Yb^{3+} (0.868 Å) dose change obviously, as revealed in Fig. 1 (c), where all diffraction peaks move to higher angle as Yb^{3+} concentration increase. Moreover, according to Scherrer formula, $D = \frac{k\lambda}{\beta \cos\theta}$, full width at half maximum of all diffraction peaks are practically unchanged, revealing the particle sizes are nearly same for all samples.

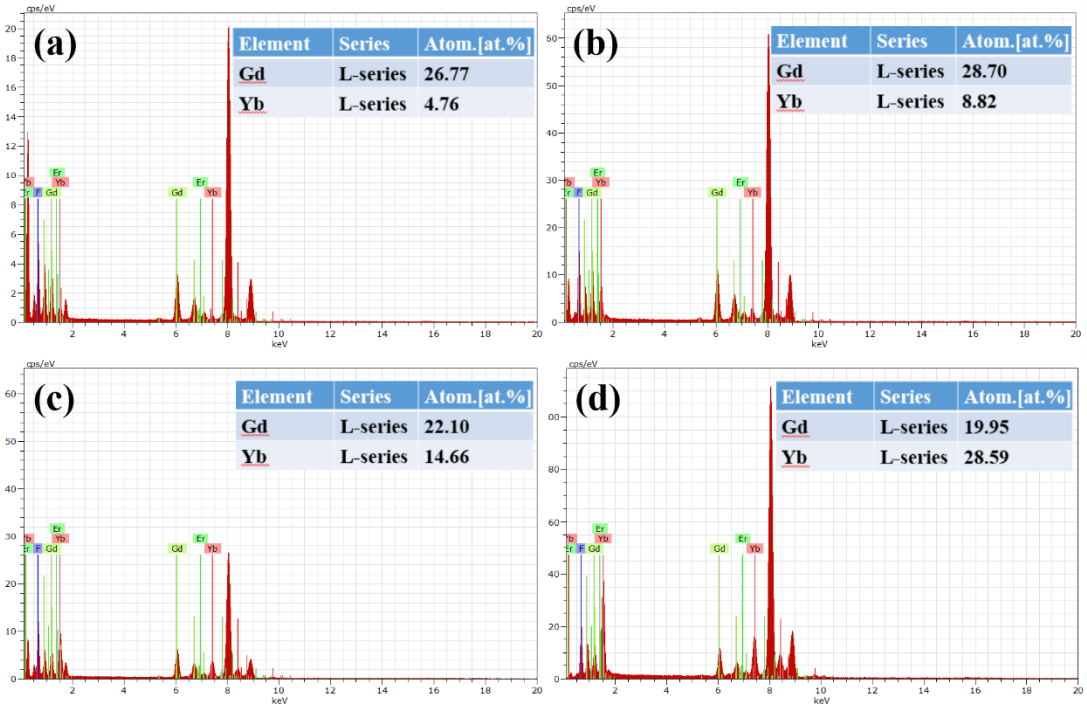

Figure S2 EDX spectra of GdF_3:2%Er^{3+} with different nominal Yb^{3+} dose: (a) 10 mol%, (b) 20 mol%, (c) 40 mol% and (d) 60 mol%.

To testify whether all the Yb^{3+} ions are doped into the crystal structure, the energy disperse X-ray spectra of all samples with different Yb^{3+} concentration are performed. The molar ratio of Yb^{3+} ions with respect to all lanthanide ions (Mol_{Yb} : Mol_{Ln}) are calculated as at[Yb]/(at[Gd] + at[Yb]) (Er^{3+} ions are ignored for its low doping concentration.): (a) 15.09%, (b) 23.51%, (c) 39.88%, (d) 58.90%. These results match quite well with nominal Yb^{3+} concentration, respectively, indicating that all Yb^{3+} ions can be considered to be completely doped into the crystal structure.

Table S1 Rate equations of five ET processes.

Mechanisms	Rate Equation (General Theory for High Yb^{3+})	Steady State RGR (N_3/N_4)[a]
ET1	$\frac{dN_1}{dt}=\omega_{21}N_2-\omega_1N_{Yb1}N_1-A_1N_1$ $\frac{dN_2}{dt}=\omega_0N_{Yb1}N_0-\omega_{21}N_2-\omega_2N_{Yb1}N_2-\omega_CN_4N_2-A_2N_2$ $\frac{dN_3}{dt}=\omega_1N_{Yb1}N_1+2\omega_CN_4N_2-A_3N_3$ $\frac{dN_4}{dt}=\omega_2N_{Yb1}N_2-\omega_CN_4N_2-A_4N_4$	$\frac{-A_4\omega_2+\omega_C\omega_0N_0}{2A_3\omega_2}+\frac{\sqrt{A_4^2\omega_2^2+6\omega_C\omega_0\omega_2A_4N_0+\omega_C^2\omega_0^2N_0^2}}{2A_3\omega_2}$
ET2	$\frac{dN_1}{dt}=\omega_{21}N_2-\omega_CN_4N_1-\omega_1N_{Yb1}N_1-A_1N_1$ $\frac{dN_2}{dt}=\omega_0N_{Yb1}N_0+\omega_CN_4N_1-\omega_{21}N_2-\omega_2N_{Yb1}N_2-A_2N_2$ $\frac{dN_3}{dt}=\omega_1N_{Yb1}N_1+\omega_CN_4N_1-A_3N_3$ $\frac{dN_4}{dt}=\omega_2N_{Yb1}N_2-\omega_CN_4N_1-A_4N_4$	$\frac{A_4\omega_{21}}{A_3\omega_2N_{Yb1}-A_3\omega_{21}}$
ET3	$\frac{dN_1}{dt}=\omega_CN_4N_0-\omega_1N_{Yb1}N_1-A_1N_1$ $\frac{dN_2}{dt}=\omega_0N_{Yb1}N_0+\omega_{2'2}N_{2'}-\omega_2N_{Yb1}N_2-A_2N_2$ $\frac{dN_2'}{dt}=\omega_CN_4N_0-\omega_{2'2}N_{2'}-A_{2'}N_{2'}$ $\frac{dN_3}{dt}=\omega_1N_{Yb1}N_1-A_3N_3$ $\frac{dN_4}{dt}=\omega_2N_{Yb1}N_2-\omega_CN_4N_0-A_4N_4$	$\frac{\omega_CN_0}{A_4}$
ET4	$\frac{dN_1}{dt}=\omega_bN_{Yb0}N_4-\omega_1N_{Yb1}N_1-A_1N_1$ $\frac{dN_2}{dt}=\omega_0N_{Yb1}N_0-\omega_2N_{Yb1}N_2-A_2N_2$ $\frac{dN_3}{dt}=\omega_1N_{Yb1}N_1-A_3N_3$ $\frac{dN_4}{dt}=\omega_2N_{Yb1}N_2-\omega_bN_{Yb0}N_4-A_4N_4$	$\frac{\omega_bN_{Yb0}}{A_4}$
ET5	$\frac{dN_1}{dt}=\omega_bN_{Yb0}N_4+\omega_{21}N_2-A_1N_1$ $\frac{dN_2}{dt}=\omega_0N_{Yb1}N_0-\omega_2N_{Yb1}N_2-\omega_{21}N_2-A_2N_2$ $\frac{dN_3}{dt}=\omega_1N_{Yb1}N_1+\omega_{43}N_4-A_3N_3$ $\frac{dN_4}{dt}=\omega_2N_{Yb1}N_2-\omega_bN_{Yb0}N_4-\omega_{43}N_4-A_4N_4$	$\frac{A_1\omega_{43}+\omega_1\omega_bN_{Yb0}N_{Yb1}}{A_1A_3}$

[a] Neglecting ETU from N_1 in ET1 and ET2 and radiation from N_1 and $N_{2(2')}$ in ET1-4.

N_1, N_2, $N_{2'}$, N_3, N_4, N_{Yb0} and N_{Yb1} are the populations of the Er^{3+} $^4I_{13/2}$, $^4I_{11/2}$, $^4I_{9/2}$, $^4F_{9/2}$, $^2H_{11/2}/^4S_{3/2}$, Yb^{3+} $^2F_{7/2}$ and $^2F_{5/2}$ manifolds, respectively. ω_0, ω_1 and ω_2 are ET parameters between Yb^{3+} $^2F_{7/2} \rightarrow {}^2F_{5/2}$ and Er^{3+} $^4I_{15/2} \rightarrow {}^4I_{11/2}$, $^4I_{13/2} \rightarrow {}^4F_{9/2}$ and $^4I_{11/2} \rightarrow {}^4F_{7/2}$, respectively. ω_{21} and ω_{43} are MPR rates from Er^{3+} $^4I_{11/2} \rightarrow {}^4I_{13/2}$ and Er^{3+} $^2H_{11/2}/^4S_{3/2} \rightarrow {}^4F_{9/2}$, respectively. ω_C is the CR rate for ET1($^4F_{7/2} + {}^4I_{11/2} \rightarrow {}^4F_{9/2} + {}^4F_{9/2}$)/ET2($^4F_{7/2} + {}^4I_{13/2} \rightarrow {}^4F_{9/2} + {}^4I_{11/2}$)/ET3($^4I_{15/2} + {}^4S_{3/2} \rightarrow {}^4I_{13/2} + {}^4I_{9/2}$). ω_b is the EBT rate to the Yb^{3+} ions. A_1, A_2, $A_{2'}$, A_3 and A_4 are radiative rates of Er^{3+} $^4I_{13/2}$, $^4I_{11/2}$, $^4I_{9/2}$, $^4F_{9/2}$ and $^2H_{11/2}/^4S_{3/2}$ manifolds, respectively. The above ET1-ET4 rate equations are proposed based on high Yb^{3+} concentrations. Hence, many radiative and nonradiative processes, such as N_1/N_2 radiative emissions, MPR processes and back-energy-transfer from Er^{3+} $^4I_{11/2} \rightarrow {}^4I_{15/2}$ transition to Yb^{3+} $^2F_{7/2} \rightarrow {}^2F_{5/2}$ transition and so on, can be neglected. As to ET5, N_1 emission is considered as major depletion of population. And MPR is considered due to the high phonon-energy groups attached to the surface of nanoparticles.

Of all rate equations, the population density of Yb^{3+} ions excited state can be generally described as following

$$\frac{dN_{Yb1}}{dt} = \sigma\rho N_{Yb0} - \sum_i \omega_i N_i N_{Yb1} - A_{Yb1} N_{Yb1} \tag{1}$$

where σ is the absorption cross-section of Yb^{3+} $^2F_{5/2}$ manifold. ρ is pump rate of the NIR laser. The incoming rate of Yb^{3+} $^2F_{5/2}$ manifold is mainly considered to be the NIR laser pumping rate. Then N_{Yb1} can be expressed as follows under steady-state condition

$$N_{Yb1} = \frac{\sigma\rho N_{Yb0}}{A_{Yb1} + \sum_i \omega_i N_i} \propto \rho \tag{2}$$

From the luminescence spectra results, we contribute the ET mechanism to ET4 or ET5, both of

which EBT process is the main mechanism to depopulate Er^{3+} green-emitting manifolds and populate Er^{3+} red-emitting manifold. To compare the two mechanisms (ET4 and ET5), the corresponding rate equations are solved and the values of N_1, N_3 and N_4 are obtained. In ET4, upconversion (UC) rate is considered as dominant depletion for $^4I_{13/2}$ manifold. In low Yb^{3+} dose samples, linear decay (LD) rate is considered as primary depletion for $^4I_{11/2}$ manifold. By solving the equations, we have

$$N_1 = \frac{\omega_0\omega_2\omega_b N_0 N_{Yb0} N_{Yb1}}{A_2\omega_1\left(A_4+\omega_b N_{Yb0}\right)} \propto \rho \tag{3}$$

$$N_3 = \frac{\omega_0\omega_2\omega_b N_0 N_{Yb0} N_{Yb1}^2}{A_2 A_3\left(A_4+\omega_b N_{Yb0}\right)} \propto \rho^2 \tag{4}$$

$$N_4 = \frac{\omega_0\omega_2 N_0 N_{Yb1}^2}{A_2\left(A_4+\omega_b N_{Yb0}\right)} \propto \rho^2 \tag{5}$$

In high Yb^{3+} dose samples, UC is considered as primary depletion for $^4I_{11/2}$ manifold. Under this situation, we have

$$N_1 = \frac{\omega_0\omega_b N_0 N_{Yb0}}{\omega_1\left(A_4+\omega_b N_{Yb0}\right)} \propto \rho^0 \tag{6}$$

$$N_3 = \frac{\omega_0\omega_b N_0 N_{Yb0} N_{Yb1}}{A_3\left(A_4+\omega_b N_{Yb0}\right)} \propto \rho^1 \tag{7}$$

$$N_4 = \frac{\omega_0 N_0 N_{Yb1}}{\left(A_4+\omega_b N_{Yb0}\right)} \propto \rho^1 \tag{8}$$

In ET5, LD is considered as dominant depletion for $^4I_{13/2}$ manifold. In low Yb^{3+} dose samples, LD is considered as primary depletion for $^4I_{11/2}$ manifold. Hence,

$$N_1 = \frac{\omega_0\omega_{21} N_0 N_{Yb1}}{A_1\left(A_2+\omega_{21}\right)} + \frac{\omega_0\omega_2\omega_b N_0 N_{Yb0} N_{Yb1}^2}{A_1\left(A_2+\omega_{21}\right)\left(A_4+\omega_{43}+\omega_b N_{Yb0}\right)} \propto a\rho^1 + b\rho^2 \tag{9}$$

$$N_3 = \frac{\omega_0\left(A_4\omega_1\omega_{21} + A_1\omega_2\omega_{43} + \omega_1\omega_{21}\omega_{43} + \omega_1\omega_{21}\omega_b N_{Yb0}\right)N_0 N_{Yb1}^2}{A_1A_3\left(A_2+\omega_{21}\right)\left(A_4+\omega_{43}+\omega_b N_{Yb0}\right)} + \frac{\omega_0\omega_1\omega_2\omega_b N_0 N_{Yb0} N_{Yb1}^3}{A_1A_3\left(A_2+\omega_{21}\right)\left(A_4+\omega_{43}+\omega_b N_{Yb0}\right)} \propto a\rho^2 + b\rho^3 \tag{10}$$

$$N_4 = \frac{\omega_0\omega_2 N_0 N_{Yb1}^2}{\left(A_2+\omega_{21}\right)\left(A_4+\omega_{43}+\omega_b N_{Yb0}\right)} \propto \rho^2 \tag{11}$$

In high Yb^{3+} dose samples, UC is considered as primary depletion for $^4I_{11/2}$ manifold. Hence

$$N_1 = \frac{\omega_0\omega_{21}N_0}{A_1+\omega_2} + \frac{\omega_0\omega_b N_0 N_{Yb0} N_{Yb1}}{A_1\left(A_4+\omega_{43}+\omega_b N_{Yb0}\right)} \propto a\rho^0 + b\rho^1 \tag{12}$$

$$N_3 = \frac{\left(A_4\omega_1\omega_{21} + A_1\omega_2\omega_{43} + \omega_1\omega_{21}\omega_{43} + \omega_1\omega_{21}\omega_b N_{Yb0}\right)\omega_0 N_0 N_{Yb1}}{A_1A_3\omega_2\left(A_4+\omega_{43}+\omega_b N_{Yb0}\right)} + \frac{\omega_0\omega_1\omega_2\omega_b N_0 N_{Yb0} N_{Yb1}^2}{A_1A_3\omega_2\left(A_4+\omega_{43}+\omega_b N_{Yb0}\right)} \propto a\rho^1 + b\rho^2 \tag{13}$$

$$N_4 = \frac{\omega_0 N_0 N_{Yb1}}{A_4+\omega_{43}+\omega_b N_{Yb0}} \propto \rho^1 \tag{14}$$

All the above results are summarized in Table 1, showing the difference between ET4 and ET5.

From the above results, the more saturation part of N_1 ($a\rho^1$ in Eq. (9) or $a\rho^0$ in Eq. (12)) and N_3 ($a\rho^2$ in Eq. (10) or $a\rho^1$ in Eq. (13)) in ET5 are due to the MPR rates, i.e., ω_{21} and ω_{43}, indicating that MPR process also contributes to the ET mechanism.

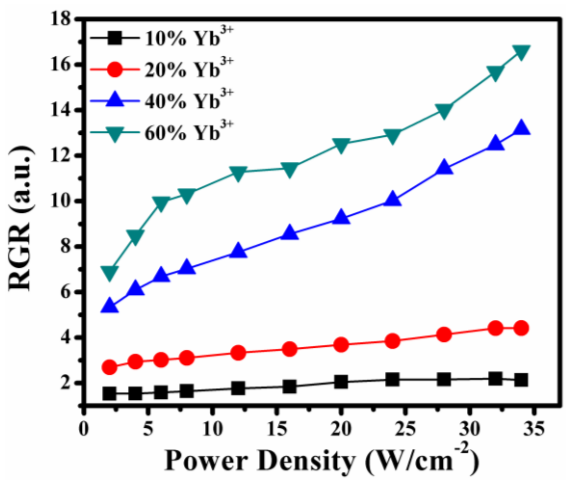

Figure S3 Excitation power density dependence of RGR for different Yb^{3+} concentration doped GdF_3:2%Er^{3+} NPs.

RGR increases faster in power dependence along with increasing Yb^{3+} concentration, demonstrating the RGR is related to two factors: Yb^{3+} concentration and pump power. This result also strengthens the point view that ET mechanism of our samples mainly conforms to ET5.

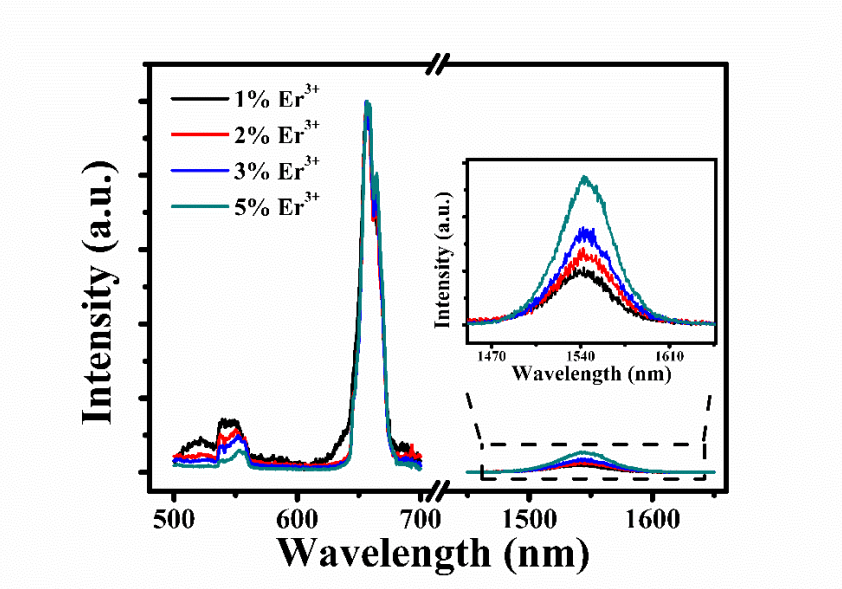

Figure S4 Normalized DS emission spectra of GdF_3:20%Yb^{3+} codoped with different Er^{3+} concentration. Inset shows the magnification of Er^{3+} $^4I_{13/2}$ NIR emission with different Er^{3+} concentration.

NIR emission relative to red emission increases along with increasing Er^{3+} concentration, which plainly demonstrates that CR process exists in our samples. Generally, CR is considered to be predominant when the average distance between activators is small enough,[1] which means the activator concentration should be adequately large. In our case, 5 mol% is large enough as the concentration quenching effect occurs when doping concentration is more than 2 mol%.[2] According to the results, the CR process may occur as Er^{3+} $^2H_{11/2}/^4S_{3/2}$ + Er^{3+} $^4I_{15/2}$ → Er^{3+} $^4I_{9/2}$ + Er^{3+} $^4I_{13/2}$, which simultaneously depopulate the green-emitting manifolds and populate NIR-emitting manifold.

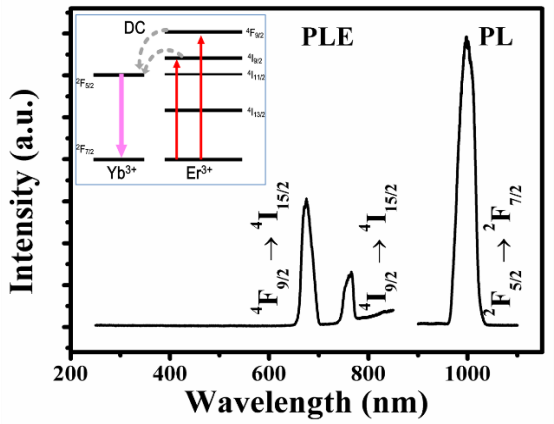

Figure S5 Excitation spectra monitored at 1 μm and emission spectra of GdF_3:20%Yb^{3+}/2%Er^{3+} NPs under 670 nm excitation. Inset shows the DC energy transfer process between Yb^{3+}-Er^{3+}.

The above spectra show that ET occur between Er^{3+} and Yb^{3+} with Yb^{3+} $^4F_{5/2}$ emission, only with Er^{3+} $^4F_{9/2}$ and Er^{3+} $^4I_{9/2}$ radiation. However, there is no excitation band of Er^{3+} $^4G_{11/2}$ manifold, suggesting that there is no Yb^{3+} NIR emission under Er^{3+} $^4G_{11/2}$ excitation.

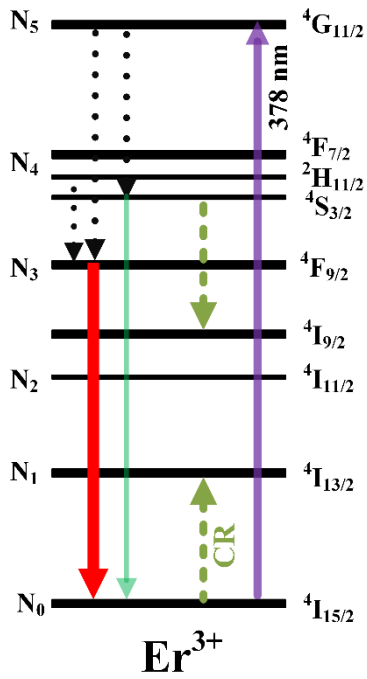

Figure S6 DS ET processes in Yb^{3+}-Er^{3+} ion pair in low dopant concentration. Solid lines, dashed lines and dotted lines represent radiative transition, cross-relaxation and multiphonon relaxation processes, respectively.

For samples with low dopant concentration, ET mechanism for DS process should not involve Yb^{3+}, which can be summarized in the above ET scheme. Er^{3+} green and red emissions are mainly due to MPR process from $^4G_{11/2}$ manifold. Er^{3+} $^4I_{13/2}$ emission is majorly due to a CR process. Hence, the corresponding rate equations can be established as follows

$$\begin{aligned}
\frac{dN_1}{dt} &= \omega_c N_0 N_4 - A_1 N_1 \\
\frac{dN_3}{dt} &= \omega_{53} N_5 + \omega_{43} N_4 - A_3 N_3 \\
\frac{dN_4}{dt} &= \omega_{54} N_5 - \omega_{43} N_4 - \omega_c N_0 N_4 - A_3 N_3 \\
\frac{dN_5}{dt} &= \sigma\rho N_5 - \omega_{54} N_5 - \omega_{53} N_5
\end{aligned} \tag{15}$$

By solving the equations, population of N_i can be obtained

$$
\begin{aligned}
N_5 &= \frac{\sigma\rho N_0}{\omega_{54}+\omega_{43}} \propto \rho \\
N_4 &= \frac{\omega_{54}}{A_4+\omega_{43}+\omega_C N_0} N_5 \propto \rho \\
N_3 &= \frac{\omega_{53}}{A_3} N_5 + \frac{\omega_{43}}{A_3} N_4 \propto \rho \\
N_1 &= \frac{\omega_C N_0}{A_1} N_4 \propto \rho
\end{aligned}
\tag{16}
$$

Thus one can find that red emission N_3 is also linear proportional to pump power, which is in good agreement with results from Figure 8.

[1] Chen, G. Y.; Somesfalean, G.; Liu, Y.; Zhang, Z. G.; Sun, Q.; Wang, F. P., Upconversion Mechanism for Two-Color Emission in Rare-Earth-Ion-Doped ZrO_2 Nanocrystals. *Phys. Rev. B* **2007**, *75*, 195204.

[2] Haase, M.; Schäfer, H., Upconverting Nanoparticles. *Angew. Chem. Int. Ed.* **2011**, *50*, 5808-5829.